processes

MDPI

Article

Optimizing Amine Functionalization of Maghemite Nanoparticles Through Controlled Hydroxylation and Silica Interlayer Engineering

Young Seo Kim and Gye Seok An *

Department of Advanced Material Engineering, Kyonggi University, 154-42 Gwanggyosan-ro, Yeongtong-gu, Suwon-si 16227, Republic of Korea; youngso7512@kyonggi.ac.kr
* Correspondence: gsmaroan@kyonggi.ac.kr; Tel.: +82-31-249-9763

Abstract: Maghemite (γ-Fe_2O_3) nanoparticles are widely used in biomedical, catalytic, and environmental applications owing to their superparamagnetic properties and surface tunability. Functionalization with primary amine groups via 3-aminopropyltriethoxysilane (APTES) is commonly employed to enable the covalent immobilization of biomolecules and other functional species. The efficiency of this silanization process depends significantly on the density of surface hydroxyl groups, which serve as reactive sites for silane coupling. In this study, the impact of acid and base pretreatments on the surface hydroxylation of γ-Fe_2O_3 nanoparticles and the subsequent APTES grafting performance was systematically evaluated. Intermediate modification using tetraethoxysilane (TEOS) was explored as a strategy to enhance silanization by forming a hydroxyl-rich silica interlayer. Fourier transform infrared spectroscopy and zeta-potential measurements were performed to assess surface chemistry and functional-group incorporation. The results indicate that acid pretreatment significantly increases the availability of reactive –OH groups, while TEOS-assisted silanization improves the uniformity and density of surface-bound amine groups. These findings highlight the critical role of surface conditioning and sequential modification in achieving the controlled and robust amine functionalization of iron oxide nanoparticles. The developed approach provides a foundation for the rational design of surface engineering protocols for high-performance magnetic nanomaterials.

Keywords: γ-Fe_2O_3 nanoparticles; surface functionalization; APTES grafting; TEOS silica interlayer; hydroxylation pretreatment

check for updates

Academic Editor: Federica Raganati

Received: 20 April 2025
Revised: 9 May 2025
Accepted: 17 May 2025
Published: 19 May 2025

Citation: Kim, Y.S.; An, G.S. Optimizing Amine Functionalization of Maghemite Nanoparticles Through Controlled Hydroxylation and Silica Interlayer Engineering. *Processes* **2025**, *13*, 1575. https://doi.org/10.3390/pr13051575

Copyright: © 2025 by the authors. Licensee MDPI, Basel, Switzerland. This article is an open access article distributed under the terms and conditions of the Creative Commons Attribution (CC BY) license (https://creativecommons.org/licenses/by/4.0/).

1. Introduction

Magnetic iron oxide nanoparticles, particularly maghemite (γ-Fe_2O_3) nanoparticles, have attracted considerable attention owing to their unique combination of superparamagnetic behavior, chemical stability, and biocompatibility [1–3]. These attributes render γ-Fe_2O_3 nanoparticles suitable for various applications, including targeted drug delivery, magnetic resonance imaging, biosensing, catalysis, and environmental remediation [4–6]. In such applications, surface chemistry plays a critical role in governing colloidal stability, dispersion behavior in various solvents, and interactions with functional molecules or biological systems. Although native iron oxide surfaces are typically rich in hydroxyl (–OH) groups, the density and chemical reactivity of these groups can vary significantly depending on the synthesis route and subsequent post-synthetic treatments. Therefore, surface functionalization strategies that enable the controlled and stable introduction of reactive

moieties are essential for tailoring the physicochemical properties of γ-Fe_2O_3 nanoparticles to meet application-specific demands.

A widely employed strategy for modifying metal oxide nanoparticle surfaces involves the use of organosilanes, which form covalent Si–O–M bonds through condensation with surface –OH groups [7]. Among these organosilanes, 3-aminopropyltriethoxysilane (APTES) is of particular interest as it introduces primary amine functionalities that serve as versatile anchoring sites for biomolecule immobilization, crosslinking reactions, or further chemical derivatization [8,9]. However, the efficiency of APTES grafting depends significantly on the surface density and accessibility of –OH groups. The insufficient availability of the –OH group can result in low grafting efficiency, non-uniform surface coverage, and the undesirable polymerization of APTES, which can lead to the formation of multilayer or aggregated structures rather than well-defined monolayers. Consequently, pre-functionalization strategies aimed at optimizing surface hydroxylation are vital for achieving consistent and effective silanization. Despite the widespread use of APTES in nanomaterials chemistry, comprehensive studies examining the relationship between surface –OH group density and silanization efficiency remain limited, particularly in the context of magnetic iron oxide systems.

Surface activation using acid or base treatments is commonly employed to enhance hydroxylation on oxide surfaces. Acidic conditions are generally believed to remove surface contaminants and increase terminal –OH group density [10,11], while basic conditions may promote the formation of bridging –OH species and alter surface roughness or porosity [12]. However, the effects of these treatments are system-dependent and influenced by parameters such as pH, treatment duration, and thermal conditions. In addition, introducing an intermediate silica layer via the hydrolysis and condensation of tetraethoxysilane (TEOS) has been proposed to improve silanization by generating a more uniform and hydroxyl-rich interface. TEOS-derived silica coatings can serve as scaffolds that facilitate the homogeneous distribution of APTES molecules and promote the formation of densely packed, stable aminosilane layers [13–15]. Moreover, SiO_2 layers derived from TEOS and APTES have been widely reported to exhibit low toxicity and excellent biocompatibility, providing a safe platform for the application of functionalized nanoparticles in biomedical and environmental fields [16,17]. However, the combined influence of acid/base pretreatments, TEOS interlayers, and subsequent APTES grafting in γ-Fe_2O_3 nanoparticle systems has not been thoroughly investigated, which has hindered the rational development of robust surface functionalization protocols.

This study investigates the effects of acid and base pretreatments on the surface –OH group density of γ-Fe_2O_3 nanoparticles and their subsequent impact on APTES-mediated amine functionalization. Furthermore, the incorporation of an intermediate TEOS-derived silica layer is explored as a strategy to enhance silanization by improving surface uniformity and –OH availability. The surface composition, grafting density, and amine incorporation are analyzed to examine the influence of each surface modification step. The novelty of this work lies in its comprehensive evaluation of sequential surface treatments, i.e., acid/base activation followed by TEOS and APTES functionalization, specifically tailored for γ-Fe_2O_3 nanoparticles. The findings provide valuable insights for the rational design of surface engineering strategies aimed at producing high-density, chemically robust amine-functionalized magnetic nanoparticles for use in advanced functional materials.

2. Experimental Procedure

2.1. Materials

Maghemite nanoparticles (γ-Fe_2O_3, 99+%, Cosmo AM & T Co., Ltd., Chungju, Republic of Korea), ammonia solution (NH_4OH, 28–30 wt% stock solution, Junsei, Tokyo, Japan),

hydrochloric acid (HCl, 0.1M, 35–37% stock solution, Samchun Chemical, Seoul, Republic of Korea), tetraethyl orthosilicate (TEOS, 95.0%, Samchun, Seoul, Republic of Korea), and APTES (99%, Sigma–Aldrich, St. Louis, MO, USA) were used.

2.2. Surface Modification of γ-Fe_2O_3 Nanoparticles

The γ-Fe_2O_3 nanoparticles (2 g) were initially subjected to a pre-washing process via ultrasonic treatment in distilled water, which was repeated three times. Thereafter, the particles were separated using an external magnet. The pre-washed nanoparticles were then introduced into a 500 mL round-bottom flask containing a 2N aqueous solution of NH_4OH or HCl. The mixture was stirred continuously at 300 rpm for 1 h while being heated to 80 °C. After the heating period, the mixture was allowed to cool naturally to room temperature while maintaining agitation. Subsequently, the nanoparticles were washed three times with distilled water and ultrasonically dispersed in 100 mL of distilled water.

2.3. Synthesis of Amino-Functionalized γ-Fe_2O_3 Nanoparticles

Amine functionalization was achieved through two distinct approaches. In the first approach, APTES was used as the sole silane precursor. γ-Fe_2O_3 nanoparticles were dispersed in a 1:1 mixture of deionized water (DIW) and ethanol via ultrasonication. Subsequently, 0.026 mol of APTES was added, and the reaction mixture was stirred at 70 °C for 48 h in a three-neck round-bottom flask. The reaction temperature was selected based on the literature to optimize the hydrolysis and condensation of APTES and was strictly maintained as a controlled parameter throughout the process. After completion, the nanoparticles were cooled to room temperature, magnetically separated, and subjected to a washing process involving one rinse with ethanol (EtOH) followed by three rinses with DIW.

In the second approach, a thin SiO_2 layer was pre-deposited onto the γ-Fe_2O_3 nanoparticles prior to APTES functionalization. Initially, γ-Fe_2O_3 nanoparticles were dispersed in a 1:1 mixture of DIW and ethanol, followed by the addition of a pre-mixed solution containing 0.2 mL of TEOS and ethanol. This mixture was vortexed for 5 min before being gradually introduced into the γ-Fe_2O_3 nanoparticle suspension using a syringe pump. The reaction was allowed to proceed under stirring at 80 °C for 18 h, which was also maintained based on prior studies to facilitate efficient TEOS hydrolysis and uniform silica deposition. Subsequently, APTES was added following the same procedure as in the first method. The resulting nanoparticles were further stirred at 70 °C for 48 h, washed, and collected for subsequent analysis.

In both approaches, reaction temperatures were consistently controlled to ensure reproducibility and to optimize silane chemistry.

2.4. Characterization

The surface functional groups of γ-Fe_2O_3 nanoparticles were analyzed using Fourier transform infrared (FT-IR) spectroscopy (IRAffinity-1S, Shimadzu, Kyoto, Japan). The surface charge variations of the prepared samples were evaluated by measuring their zeta-potential values using dynamic light scattering (Zetasizer Nano ZSP, Malvern Instruments, Westborough, MA, USA). The magnetic properties of γ-Fe_2O_3 and amine-functionalized γ-Fe_2O_3 nanoparticles were characterized using a vibrating sample magnetometer (VSM; Lake Shore 7400, Lake Shore Cryotronics, Inc., Westerville, OH, USA) in the field range of −10 to +10 kOe. The particle size and morphological characteristics were examined via transmission electron microscopy (TEM; Tecnai, FEI, Eindhoven, The Netherlands).

3. Results and Discussion

Figure 1 presents the FT-IR spectra used to analyze the changes in functional groups resulting from the surface modification of γ-Fe_2O_3 nanoparticles. The measurements were performed using the KBr pellet technique, in which the sample was homogenized with potassium bromide and compressed into a transparent pellet. In this analysis, the chemical modifications of as-received γ-Fe_2O_3 and γ-Fe_2O_3 nanoparticles surface-treated in acidic and basic environments using HCl and NH_4OH, respectively, were investigated. A broad absorption band was observed around 570 cm^{-1} in all the samples, which is attributed to Fe–O stretching vibrations [18].

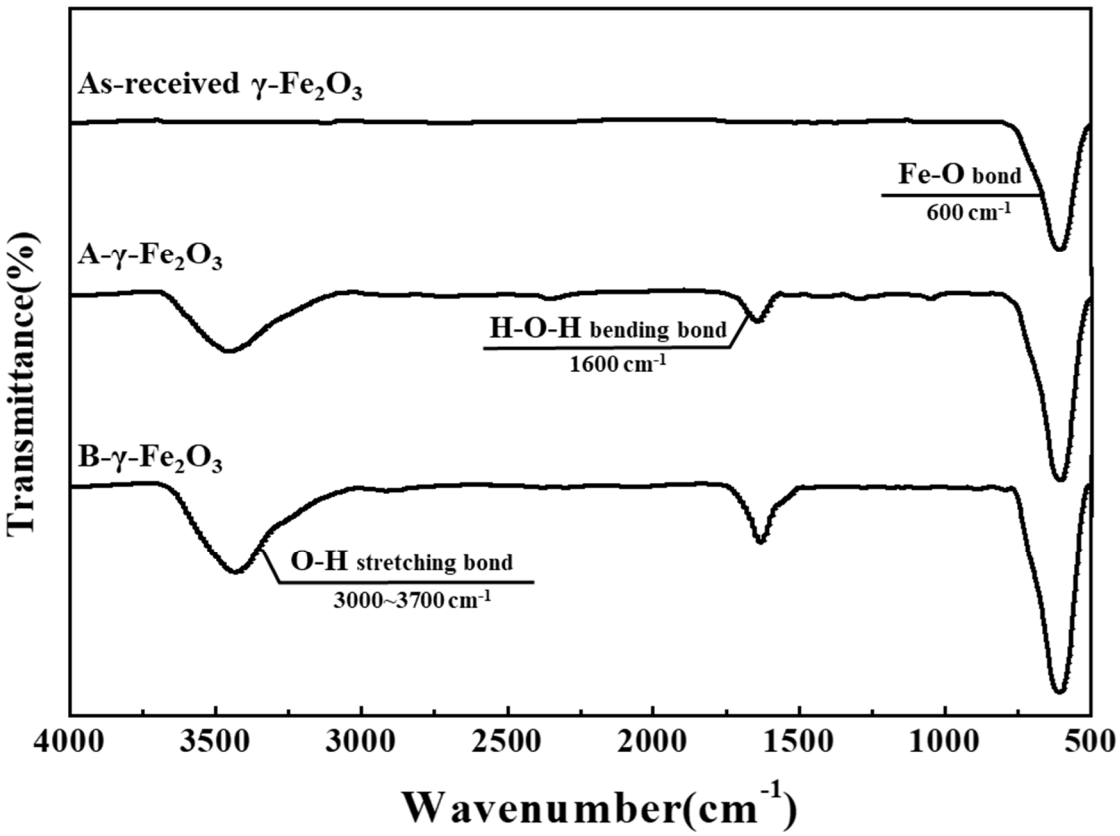


Figure 1. FT-IR spectra of as-received γ-Fe_2O_3, A-γ-Fe_2O_3, and B-γ-Fe_2O_3.

In the FT-IR spectra of the Acid-γ-Fe_2O_3 (A-γ-Fe_2O_3) and Base-γ-Fe_2O_3 (B-γ-Fe_2O_3) samples, a broad O–H stretching vibration peak was observed in the region of 3000–3700 cm^{-1} [19], along with an H–O–H bending vibration peak around 1600 cm^{-1} [20]. This indicates an increase in the density of –OH groups and adsorbed water molecules on the surface of γ-Fe_2O_3 nanoparticles due to surface modification. The HCl and NH_4OH treatments effectively altered the surface of γ-Fe_2O_3 nanoparticles, promoting the formation of –OH groups and the adsorption of water molecules, which increased the intensities of the O–H and H–O–H vibration peaks.

Notably, the B-γ-Fe_2O_3 sample treated with NH_4OH exhibited stronger O–H and H–O–H peaks than the A-γ-Fe_2O_3 sample treated with HCl. This is because NH_4OH, a strong base, provides OH^- ions, facilitating hydroxylation reactions on the γ-Fe_2O_3 surface and altering the surface charge to a more negative state, which induces the additional adsorption of water molecules [21]. In contrast, HCl provides an acidic environment, reacting with some of the Fe–OH groups on the surface, which may partially suppress –OH group formation through dehydration-condensation or Cl^- substitution [22]. Because of

these mechanistic differences, NH_4OH treatment is found to induce the greater formation of –OH groups on the surface of γ-Fe_2O_3 nanoparticles than HCl treatment.

Overall, the surface modification process was demonstrated to facilitate the adsorption of –OH groups and water molecules.

Figure 2 presents the zeta potential and polydispersity index (PDI) values measured to evaluate the dispersion stability of the as-received γ-Fe_2O_3 nanoparticles, as well as the surface-modified A-γ-Fe_2O_3 and B-γ-Fe_2O_3 nanoparticles treated with HCl and NH_4OH, respectively. All samples were dispersed in deionized water (DIW) prior to measurement. The measurement results indicated that the as-received γ-Fe_2O_3 nanoparticles had a zeta potential of -1.6 ± 2 mV and a PDI of 0.824 ± 0.13. This suggested that the weak electrostatic repulsion between γ-Fe_2O_3 nanoparticles led to aggregation, resulting in a broad particle-size distribution (PSD) and a high PDI value. The measured pH of the dispersion was 6.1.

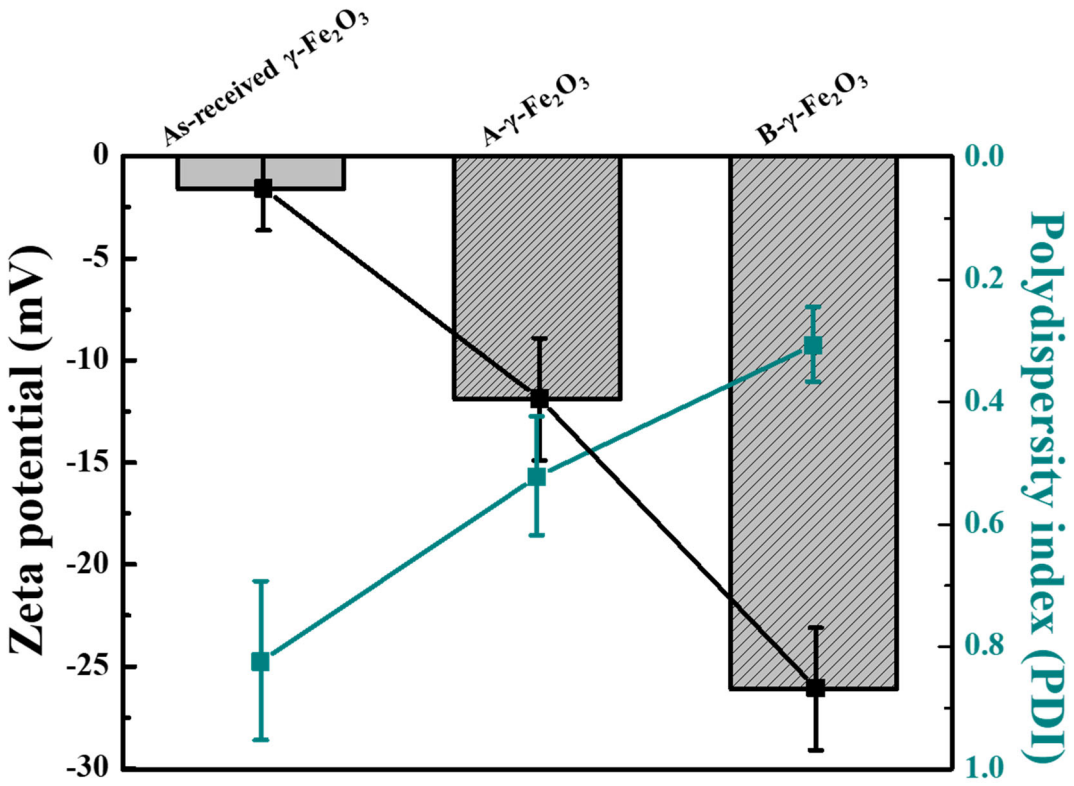


Figure 2. Zeta potential and PDI values of as-received γ-Fe_2O_3, A-γ-Fe_2O_3, and B-γ-Fe_2O_3.

In contrast, the surface-modified nanoparticles treated with HCl and NH_4OH exhibited zeta-potential values of -11.9 ± 3 mV and -26.1 ± 3 mV, respectively, with corresponding PDI values of 0.522 ± 0.097 and 0.367 ± 0.061. The pH values of the dispersions were measured to be 4.3 for the acid-treated sample and 9.4 for the base-treated sample. Compared with as-received γ-Fe_2O_3, the surface-modified nanoparticles exhibited lower PDI values. This is attributed to the increased electrostatic repulsion between particles due to surface modification, which enhances the dispersion stability.

Notably, the B-γ-Fe_2O_3 nanoparticles treated with NH_4OH exhibited a higher absolute zeta-potential value and a lower PDI value than the A-γ-Fe_2O_3 nanoparticles treated with HCl. Consistent with the FT-IR spectral analysis in Figure 1, this suggests that NH_4OH treatment led to the formation of a larger number of –OH groups on the surface, which increased the surface charge and electrostatic repulsion between particles and ultimately improved the dispersion stability. Therefore, base treatment is considered more effective for enhancing the dispersion stability of nanoparticles than acid treatment.

Figure 3 visually represents the surface modification of B-γ-Fe_2O_3 nanoparticles through alkaline treatment followed by functionalization using TEOS and APTES. Upon treatment with NH_4OH, –OH groups are introduced onto the surface of the B-γ-Fe_2O_3 nanoparticles. Subsequently, the nanoparticles undergo amine functionalization through two different approaches: (1) direct functionalization with APTES and (2) sequential treatment with TEOS followed by APTES functionalization.

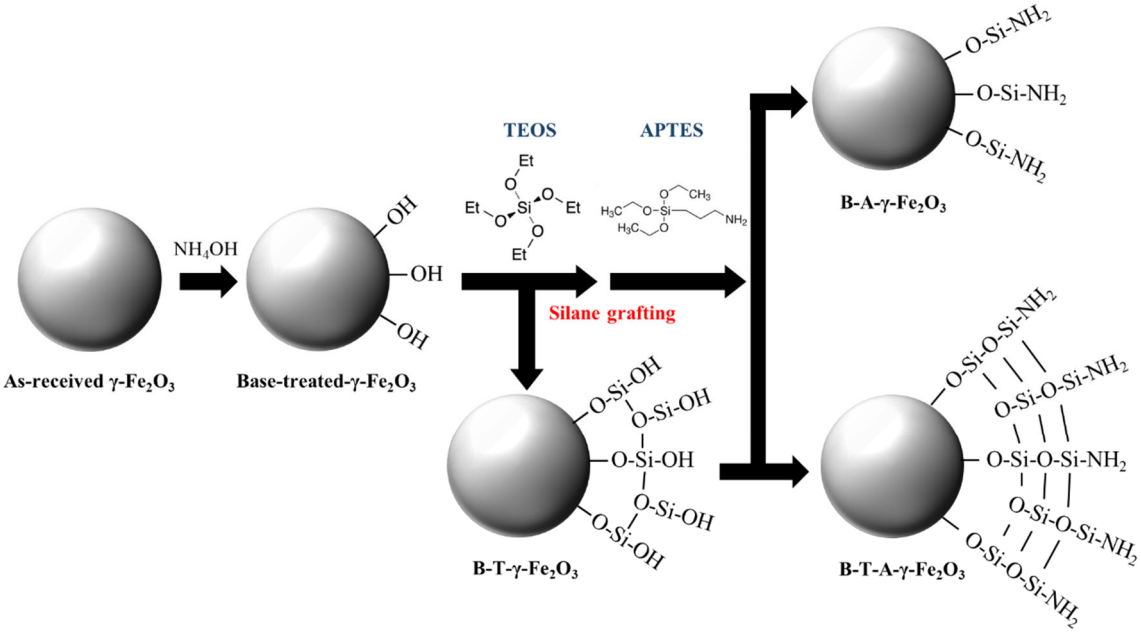


Figure 3. Schematic of surface-modified and amine-functionalized γ-Fe_2O_3 nanoparticles.

In the first approach, APTES is directly introduced onto the surface of B-γ-Fe_2O_3 nanoparticles. The ethoxy (–OCH_2CH_3) groups of APTES undergo hydrolysis in the presence of water, leading to the formation of silanol (Si–OH) groups. These Si–OH groups react with the –OH groups present on the nanoparticle surface via condensation reactions, forming Si-O-Si bonds through silane grafting [23]. This results in the introduction of NH_2 functional groups in a monolayer configuration. However, owing to the limited availability of active sites on the nanoparticle surface, the density of amine functional groups incorporated through this method is relatively low.

Conversely, in the second approach, TEOS is introduced before APTES functionalization. During the hydrolysis of TEOS, ethanol (C_2H_5OH) is eliminated, forming Si–OH groups. The generated $Si(OH)_4$ molecules react with surface –OH groups on B-γ-Fe_2O_3, forming Fe–O–$Si(OH)_3$ bonds. This is followed by condensation reactions, facilitating the development of a three-dimensional SiO_2 network on the nanoparticle surface [24]. The increased density of Si–OH groups resulting from this process provides a larger number of active sites for subsequent APTES attachment. When APTES is introduced, its hydrolysis and condensation reactions with terminal Si–OH groups of the preformed SiO_2 network enable the formation of robust chemical bonds, increasing the density of amine (-NH_2) functional groups on the nanoparticle surface.

According to these findings, the pretreatment of B-γ-Fe_2O_3 nanoparticles with TEOS prior to APTES functionalization is a more effective strategy for introducing amine groups than direct APTES grafting. The formation of a three-dimensional SiO_2 network enhances the available binding sites, increasing the attachment density of APTES and optimizing the surface modification efficiency.

Figure 4 presents the FT-IR spectral analysis of γ-Fe_2O_3 nanoparticles before and after TEOS and APTES treatments, highlighting the chemical modifications at the nanoparticle surface. The functional group variations in base-treated γ-Fe_2O_3 (B-T-γ-Fe_2O_3) nanoparticles following TEOS treatment were examined, revealing that the Fe-O bond remained intact. This observation suggests that TEOS treatment does not alter the fundamental structural characteristics of γ-Fe_2O_3 nanoparticles. Furthermore, new peaks corresponding to Si-O-Si bonds appeared at 1220 and 1070 cm^{-1} [25], confirming the successful formation of an SiO_2 shell on the nanoparticle surface after NH_4OH treatment. The FT-IR spectra also exhibited an increased intensity of –OH and H–O–H vibration peaks following TEOS treatment. This is attributed to the hydrolysis and condensation reactions of TEOS, which led to the formation of additional Si-OH groups on the surface [26]. These Si-OH groups are likely to form hydrogen bonds with pre-existing –OH groups on the γ-Fe_2O_3 surface or facilitate water-molecule adsorption, increasing the O–H stretching and H-O-H bending vibration intensities.

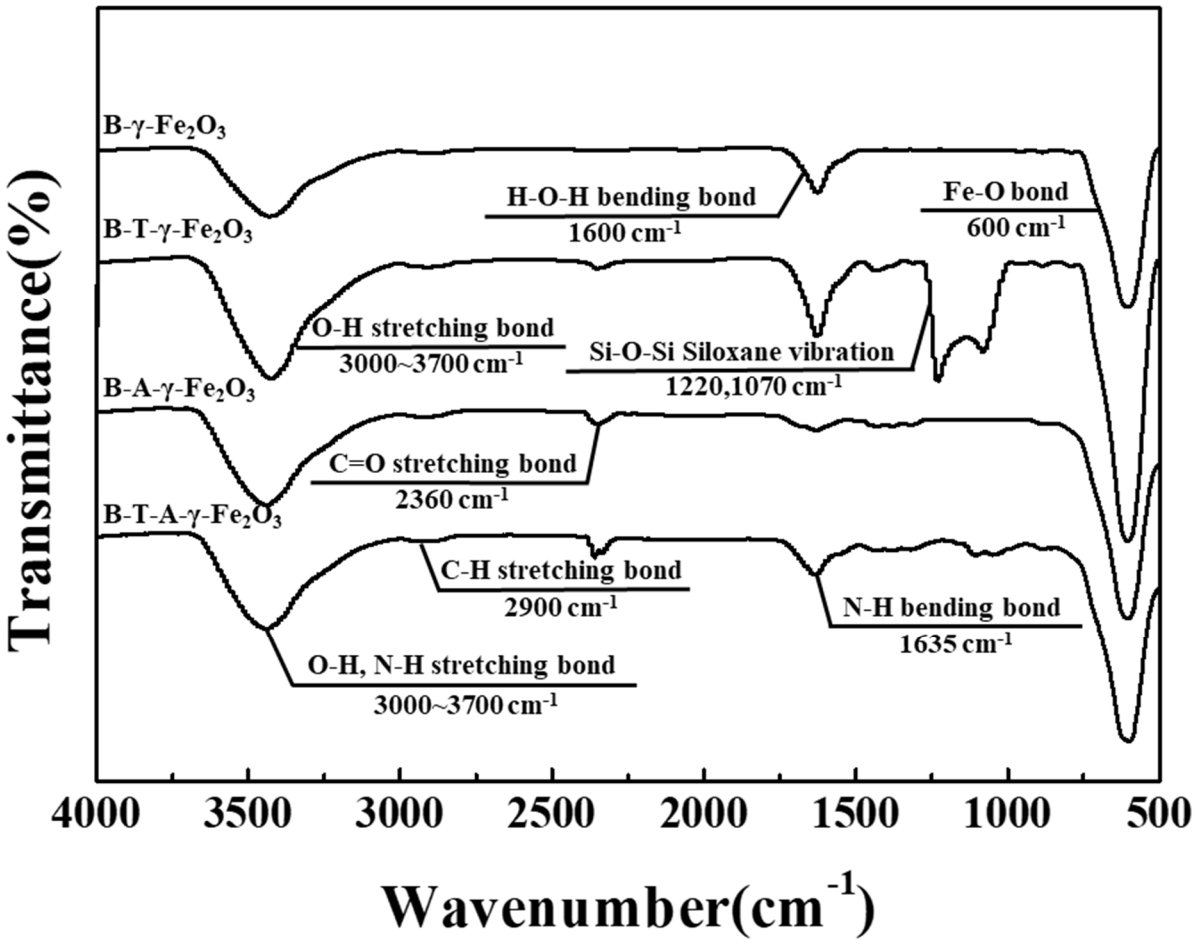


Figure 4. FT-IR spectra of B-A-γ-Fe_2O_3, B-T-γ-Fe_2O_3, B-A-γ-Fe_2O_3, and B-T-A-γ-Fe_2O_3.

Additionally, FT-IR analysis of base-APTES γ-Fe_2O_3 (B-A-γ-Fe_2O_3) and base-TEOS-APTES γ-Fe_2O_3 (B-T-A-γ-Fe_2O_3) nanoparticles confirmed the introduction of amine functionalities. Distinct absorption peaks were observed at 3000–3700 cm^{-1} (N–H stretching vibration), approximately 2900 cm^{-1} (C–H stretching vibration), and 1635 cm^{-1} (N–H bending vibration), indicating the successful functionalization of the nanoparticle surface [27–29]. These results confirm that APTES, an organosilane compound with a terminal amine (-NH_2) group, chemically bonded to the nanoparticle surface via covalent interactions.

To provide a comparative assessment of amine group incorporation, the FTIR absorption bands corresponding to N–H bending (~1635 cm^{-1}) and C–H stretching (~2900 cm^{-1}) were qualitatively evaluated relative to the Fe–O stretching band at 570 cm^{-1}. The B-T-A-γ-Fe_2O_3 sample exhibited noticeably stronger N–H and C–H signals than the B-A-γ-Fe_2O_3 sample, indicating a higher level of surface amine functionalization. Although not quantitatively determined, this relative enhancement supports the conclusion that the TEOS-mediated silica interlayer promotes more effective and homogeneous APTES grafting.

Notably, in the B-T-A-γ-Fe_2O_3 sample, the SiO_2 shell formed during TEOS treatment facilitated siloxane bond formation with APTES, leading to the retention of the Si–O–Si peaks at 1220 and 1070 cm^{-1}. Simultaneously, the intensities of FT-IR peaks associated with amine functional groups were significantly increased. This suggests that TEOS treatment not only provides an abundance of Si-OH groups on the surface but also promotes strong APTES binding, facilitating a higher degree of amine functionalization on the nanoparticles.

In conclusion, TEOS treatment preserves the intrinsic properties of γ-Fe_2O_3 while introducing a thin SiO_2 layer that enhances surface –OH and H–O–H bonding characteristics. Furthermore, the pre-deposited SiO_2 layer improves the stability and uniformity of APTES functionalization, leading to an increase in surface hydrophilicity and a more homogeneous amine group distribution. These findings suggest that the combined TEOS and APTES treatment serves as an effective strategy for surface modification, significantly improving the functionality of γ-Fe_2O_3 nanoparticles for potential applications.

Figure 5 presents TEM images used to analyze the morphological characteristics of γ-Fe_2O_3 nanoparticles, including the particle size and surface structure. The images correspond to (a) as-received γ-Fe_2O_3, (b) base-treated B-A-γ-Fe_2O_3 nanoparticles modified with NH_4OH, (c) B-T-A-γ-Fe_2O_3 nanoparticles further coated with TEOS, and (d) B-T-A-γ-Fe_2O_3 nanoparticles subjected to additional amine functionalization using APTES. The average particle size for all the samples was measured to be in the range of approximately 270–290 nm, indicating that the NH_4OH-based base treatment, TEOS coating, and APTES functionalization processes were successfully conducted without causing structural degradation of the γ-Fe_2O_3 core.

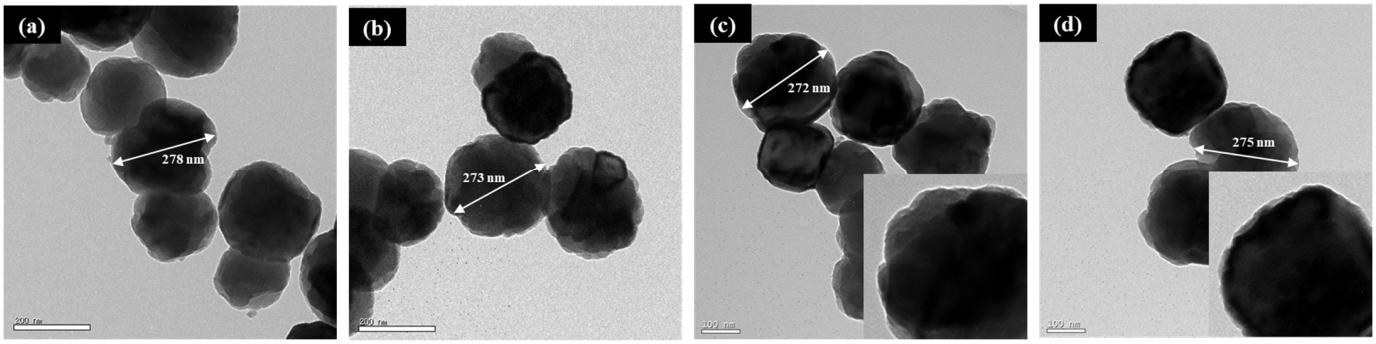


Figure 5. TEM images of (**a**) as-received γ-Fe_2O_3, (**b**) B-A-γ-Fe_2O_3, (**c**) B-T-γ-Fe_2O_3, and (**d**) B-T-A-γ-Fe_2O_3.

Notably, the TEM images in Figure 5c,d show no distinct shell structure or additional phase-separated materials, despite the application of TEOS and APTES treatments. This suggests that TEOS and APTES were adsorbed onto the nanoparticle surface in an ultrathin and uniform manner, forming SiO_2 and organic layers that were not sufficiently thick to be distinctly identified via TEM analysis. Additionally, the nanoparticles retained their spherical or quasi-spherical morphology even after surface modifications, indicating that the modification processes had minimal impact on the morphological stability of γ-Fe_2O_3 nanoparticles.

Consequently, the results confirm that the base treatment, TEOS coating, and amine functionalization processes applied in this study effectively modified the nanoparticle surface without inducing structural changes in the γ-Fe_2O_3 core.

Figure 6a presents the zeta-potential measurements of B-A-γ-Fe_2O_3, B-T-γ-Fe_2O_3, and B-T-A-γ-Fe_2O_3 nanoparticles after amine functionalization via APTES treatment, indicating their dispersion stability. All samples were dispersed in deionized water (DIW), and the pH values of the respective dispersions were measured to be 7.3 for B-A-γ-Fe_2O_3, 10.0 for B-T-γ-Fe_2O_3 and 4.9 for B-T-A-γ-Fe_2O_3. The measured zeta-potential values were 7.1 ± 2 mV for B-A-γ-Fe_2O_3, −48.3 ± 2 mV for B-T-γ-Fe_2O_3, and 35.4 ± 3 mV for B-T-A-γ-Fe_2O_3. These variations are primarily attributed to TEOS treatment, which facilitates the effective adsorption of APTES amine groups onto the γ-Fe_2O_3 surface. Notably, the absolute zeta-potential value of B-T-A-γ-Fe_2O_3 increased more than threefold compared with that of B-A-γ-Fe_2O_3, indicating a significant enhancement in dispersion stability. Furthermore, the increase in the absolute zeta-potential value was directly correlated with the higher concentration of positively charged amine groups. The positive shift in zeta potential for B-T-A-γ-Fe_2O_3 confirms the successful incorporation of a larger number of amine groups, which aligns with the higher N–H bending peak intensity observed in the FT-IR spectrum of Figure 4. These results collectively suggest that TEOS serves as a precursor for forming a thin SiO_2 layer on the γ-Fe_2O_3 surface, which subsequently facilitates siloxane bonding with APTES, leading to more efficient amine functionalization. The findings indicate that TEOS treatment significantly improves the dispersion stability of amine-functionalized γ-Fe_2O_3 nanoparticles.

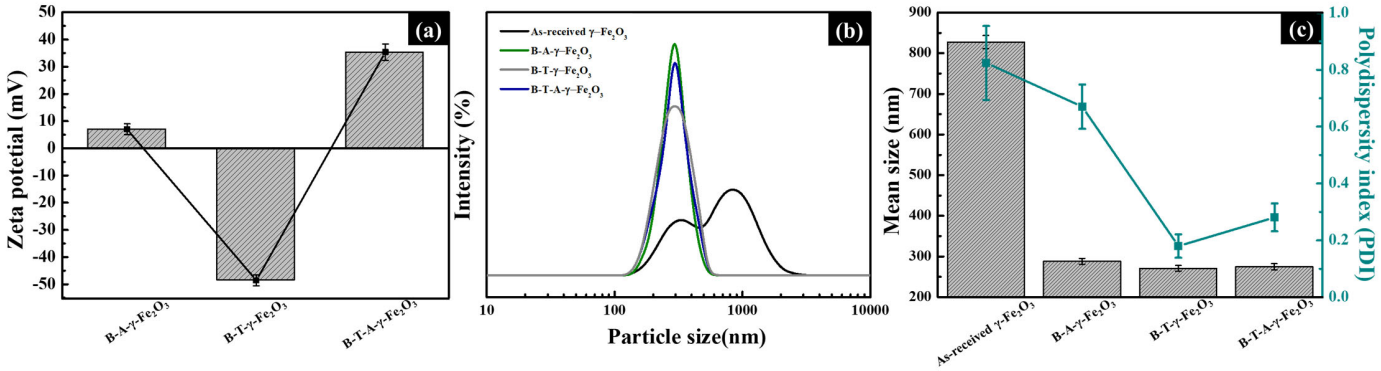


Figure 6. (**a**) Zeta potential, (**b**) PSD, and (**c**) mean size and PDI of as-received γ-Fe_2O_3, B-A-γ-Fe_2O_3, B-T-γ-Fe_2O_3, and B-T-A-γ-Fe_2O_3.

Figure 6b,c illustrate the PSD, mean particle size, and PDI of as-received γ-Fe_2O_3 and surface-modified nanoparticles. The as-received γ-Fe_2O_3 nanoparticles exhibited a bimodal distribution with peaks at approximately 370 and 990 nm, with an average particle size of 827.4 ± 16.4 nm and a PDI of 0.824 ± 0.13. This significantly larger size compared with the individual particles observed in the TEM images (Figure 5) suggests aggregation due to poor dispersion stability. In contrast, the average particle sizes and PDIs of the surface-modified nanoparticles, including B-A-γ-Fe_2O_3, B-T-γ-Fe_2O_3, and B-T-A-γ-Fe_2O_3, were measured as 289.1 ± 7.3 nm and 0.67 ± 0.078, 270.9 ± 6.9 nm and 0.18 ± 0.031, and 274.6 ± 7.6 nm and 0.281 ± 0.039, respectively. These values closely match those observed in the TEM analysis, confirming that surface modification effectively prevents aggregation.

Additionally, the changes in the PSD patterns indicate that surface modification enhances electrostatic repulsion between particles, suppressing aggregation and leading to a transition from a bimodal to a monomodal distribution. In Figure 6a, the significantly higher absolute zeta-potential values of B-T-γ-Fe_2O_3 and B-T-A-γ-Fe_2O_3 compared with

B-A-γ-Fe_2O_3 corroborate their superior dispersion stability. This is also reflected in the PSD graphs, where these samples exhibit narrower and more defined peaks.

In conclusion, the combined treatments of NH_4OH, TEOS, and APTES effectively improve the surface characteristics and dispersion stability of γ-Fe_2O_3 nanoparticles while maintaining the core particle size without significant alteration.

Figure 7 presents the VSM analysis results conducted to evaluate the effect of APTES-based amine functionalization on the magnetic properties of γ-Fe_2O_3 nanoparticles. The magnetic hysteresis curves for all the samples exhibited a linear form with no residual magnetization or coercivity, indicating that the synthesized nanoparticles retained their superparamagnetic properties.

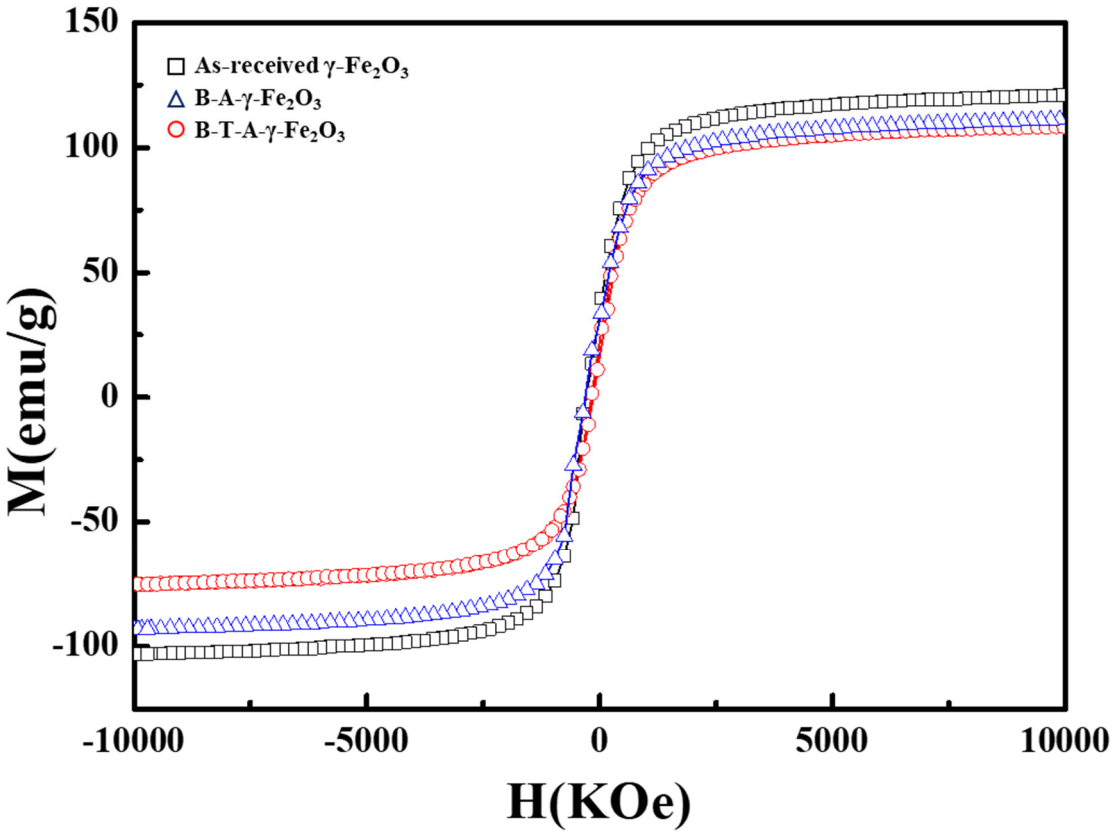


Figure 7. Magnetization curves of as-received γ-Fe_2O_3, B-A-γ-Fe_2O_3, and B-T-A-γ-Fe_2O_3.

The as-received γ-Fe_2O_3 nanoparticles exhibited a high saturation magnetization (M_s) value of 121.48 emu/g. After surface modification with APTES, the M_s values of B-A-γ-Fe_2O_3 and B-T-A-γ-Fe_2O_3 samples were slightly reduced to 111.24 and 109.81 emu/g, respectively.

This reduction in Ms is not primarily attributed to the surface-bound functional groups, which are present only in trace amounts and thus exert negligible influence on the overall magnetic response. Rather, it may be attributed to two main factors: (1) improved dispersion stability of the surface-modified particles, which minimizes magnetic interactions among aggregated particles during VSM measurement, and (2) minor structural changes such as surface etching or partial reduction in magnetic core volume caused by acid/base and silanization treatments.

However, all the samples maintained their superparamagnetic properties, suggesting that the surface modification did not significantly impair the magnetic characteristics of γ-Fe_2O_3 nanoparticles. Consequently, APTES amine functionalization is considered to have only a minor impact on the magnetic properties of γ-Fe_2O_3 nanoparticles.

4. Conclusions

In this study, the effects of sequential surface modification on γ-Fe_2O_3 nanoparticles were systematically investigated with the aim of achieving high-density and uniform amine functionalization via APTES. The results clearly demonstrated that surface pretreatment using NH_4OH significantly increased the density of surface –OH groups compared with HCl treatment, as confirmed by FT-IR spectroscopy and zeta-potential measurements. The enhanced hydroxylation led to improved dispersion stability and provided more reactive sites for subsequent silanization. Moreover, the introduction of an intermediate silica layer through TEOS hydrolysis and condensation was shown to further amplify surface functionality. The formation of Si–OH-rich networks on the nanoparticle surface not only facilitated APTES attachment but also promoted the development of a densely packed and stable aminosilane layer. This was substantiated by the increased intensities of characteristic N–H and C–H vibrations in FT-IR spectra and the significant positive shift in zeta potential.

Morphological analysis using TEM confirmed that the surface modification processes, including base activation, TEOS coating, and APTES functionalization, did not alter the spherical structure or size of the γ-Fe_2O_3 core, thus preserving the intrinsic particle characteristics. PSD and PDI values further indicated a marked improvement in monodispersity and colloidal stability, particularly for the samples subjected to TEOS-assisted APTES grafting. Additionally, VSM measurements revealed that the magnetic properties of γ-Fe_2O_3 nanoparticles were retained after modification, with only a minor decrease in saturation magnetization attributed to the non-magnetic silica and organic layers on the surface.

Overall, this work presents a rational and effective strategy for tailoring the surface chemistry of γ-Fe_2O_3 nanoparticles through the combined use of hydroxylation pretreatment and silica interlayer engineering. The approach allows for enhanced control over amine group density, surface uniformity, and dispersion stability without compromising magnetic functionality, offering a reliable platform for developing high-performance magnetic nanomaterials with application-specific surface properties.

Author Contributions: Conceptualization, methodology, validation, formal analysis, investigation, data curation, writing—original draft preparation, and visualization, Y.S.K.; writing—review and editing, resources, and supervision, G.S.A. All authors have read and agreed to the published version of the manuscript.

Funding: This work was supported by Kyonggi University Research Grant 2022.

Data Availability Statement: Data are contained within the article.

Conflicts of Interest: The author declares no conflicts of interest.

References

1. Li, J.; Hu, J.; Ma, C.; Wang, Y.; Wu, C.; Huang, J.; Xing, B. Uptake, translocation and physiological effects of magnetic iron oxide (γ-Fe_2O_3) nanoparticles in corn (*Zea mays* L.). *Chemosphere* **2016**, *159*, 326–334. [CrossRef] [PubMed]
2. Wen, B.; Li, J.; Lin, Y.; Liu, X.; Fu, J.; Miao, H.; Zhang, Q. A novel preparation method for γ-Fe2O3 nanoparticles and their characterization. *Mater. Chem. Phys.* **2011**, *128*, 35–38. [CrossRef]
3. Prasad, N.K.; Panda, D.; Singh, S.; Mukadam, M.D.; Yusuf, S.M.; Bahadur, D. Biocompatible suspension of nanosized γ-Fe_2O_3 synthesized by novel methods. *J. Appl. Phys.* **2005**, *97*, 10Q903. [CrossRef]
4. Cao, S.W.; Zhu, Y.J.; Ma, M.Y.; Li, L.; Zhang, L. Hierarchically nanostructured magnetic hollow spheres of Fe_3O_4 and γ-Fe_2O_3: Preparation and potential application in drug delivery. *J. Phys. Chem. C* **2008**, *112*, 1851–1856. [CrossRef]
5. Yang, B.; Zhang, Y.; Sun, L.; Wang, J.; Zhao, Z.; Huang, Z.; Qin, Y. Modulated ultrasmall γ-Fe_2O_3 nanocrystal assemblies for switchable magnetic resonance imaging and photothermal-ferroptotic-chemical synergistic cancer therapy. *Adv. Funct. Mater.* **2023**, *33*, 2211251. [CrossRef]
6. Piraman, S.; Sundar, S.; Mariappan, R.; Kim, Y.Y.; Min, K. Nanospheres and nanoleaves of γ-Fe_2O_3 architecturing for magnetic and biomolecule sensing applications. *Sens. Actuators B Chem.* **2016**, *234*, 386–394. [CrossRef]

7. Goyal, S. Silanes: Chemistry and applications. *J. Indian Prosthodont. Soc.* **2006**, *6*, 14–18. [CrossRef]
8. Gunda, N.S.K.; Singh, M.; Norman, L.; Kaur, K.; Mitra, S.K. Optimization and characterization of biomolecule immobilization on silicon substrates using (3-aminopropyl) triethoxysilane (APTES) and glutaraldehyde linker. *Appl. Surf. Sci.* **2014**, *305*, 522–530. [CrossRef]
9. Liu, Y.; Bai, Z.; Lin, G.; Wang, L.; Xu, X.; He, L.; Liu, X. Covalent cross-linking mediated TA-APTES NPs to construct a high-efficiency GO composite membrane for dye/salt separation. *Appl. Surf. Sci.* **2022**, *584*, 152595. [CrossRef]
10. Anttila, O.J.; Tilli, M.V. Metal contamination removal on silicon wafers using dilute acidic solutions. *J. Electrochem. Soc.* **1992**, *139*, 1751. [CrossRef]
11. Chatterjee, A.; Iwasaki, T.; Ebina, T.; Tsuruya, H.; Kanougi, T.; Oumi, Y.; Miyamoto, A. Effects of structural characteristics of zeolites on the properties of their bridging and terminal hydroxyl groups. *Appl. Surf. Sci.* **1998**, *130*, 555–560. [CrossRef]
12. Kazansky, V.B.; Serykh, A.I.; Semmer-Herledan, V.; Fraissard, J. Intensities of OH IR stretching bands as a measure of the intrinsic acidity of bridging hydroxyl groups in zeolites. *Phys. Chem. Chem. Phys.* **2003**, *5*, 966–969. [CrossRef]
13. Pilipavicius, J.; Kaleinikaite, R.; Pucetaite, M.; Velicka, M.; Kareiva, A.; Beganskiene, A. Controllable formation of high density SERS-active silver nanoprism layers on hybrid silica-APTES coatings. *Appl. Surf. Sci.* **2016**, *377*, 134–140. [CrossRef]
14. Aharipour, N.; Khachatourian, A.M.; Nemati, A. Synthesis of Fe_3O_4@ m-SiO_2 Nanocomposites Using Rice Husk Ash Derived SiO_2. *Iran. J. Mater. Sci. Eng.* **2024**, *21*, 119–128.
15. Chircov, C.; Matei, M.F.; Neacșu, I.A.; Vasile, B.S.; Oprea, O.C.; Croitoru, A.M.; Bărbuceanu, F. Iron oxide–silica core–shell nanoparticles functionalized with essential oils for antimicrobial therapies. *Antibiotics* **2021**, *10*, 1138. [CrossRef]
16. Rashti, A.; Yahyaei, H.; Firoozi, S.; Ramezani, S.; Rahiminejad, A.; Karimi, R.; Ghanbari, H. Development of novel biocompatible hybrid nanocomposites based on polyurethane-silica prepared by sol gel process. *Mater. Sci. Eng. C* **2016**, *69*, 1248–1255. [CrossRef]
17. Javid, A.; Ahmadian, S.; Saboury, A.A.; Kalantar, S.M.; Rezaei-Zarchi, S.; Shahzad, S. Biocompatible APTES–PEG modified magnetite nanoparticles: Effective carriers of antineoplastic agents to ovarian cancer. *Appl. Biochem. Biotechnol.* **2014**, *173*, 36–54. [CrossRef]
18. Wu, G.; Tan, X.; Li, G.; Hu, C. Effect of preparation method on the physical and catalytic property of nanocrystalline Fe_2O_3. *J. Alloys Compd.* **2010**, *504*, 371–376. [CrossRef]
19. Yu, X.; Liu, S.; Yu, J. Superparamagnetic γ-Fe_2O_3@ SiO_2@ TiO_2 composite microspheres with superior photocatalytic properties. *Appl. Catal. B Environ.* **2011**, *104*, 12–20. [CrossRef]
20. Malega, F.; Indrayana, I.P.T.; Suharyadi, E. Synthesis and characterization of the microstructure and functional group bond of fe3o4 nanoparticles from natural iron sand in Tobelo North Halmahera. *J. Ilm. Pendidik. Fis. Al-Biruni* **2018**, *7*, 13–22. [CrossRef]
21. Kegl, T.; Ban, I.; Lobnik, A.; Košak, A. Synthesis and characterization of novel γ-Fe_2O_3-NH_4OH@ SiO_2 (APTMS) nanoparticles for dysprosium adsorption. *J. Hazard. Mater.* **2019**, *378*, 120764. [CrossRef] [PubMed]
22. Zhou, W.; Niu, S.; Wang, J.; Li, Y.; Han, K.; Wang, Y.; Wang, Y.; Lu, C.; Zhu, Y. Study on the adsorption and oxidation mechanism of mercury by HCl over γ-Fe_2O_3 catalyst. *J. Fuel Chem. Technol.* **2021**, *49*, 1716–1723. [CrossRef]
23. Majoul, N.; Aouida, S.; Bessaïs, B. Progress of porous silicon APTES-functionalization by FTIR investigations. *Appl. Surf. Sci.* **2015**, *331*, 388–391. [CrossRef]
24. Cai, Y.; Hou, P.; Duan, C.; Zhang, R.; Zhou, Z.; Cheng, X.; Shah, S. The use of tetraethyl orthosilicate silane (TEOS) for surface-treatment of hardened cement-based materials: A comparison study with normal treatment agents. *Constr. Build. Mater.* **2016**, *117*, 144–151. [CrossRef]
25. Geng, A.Y.; Ding, G.Q.; She, H.H.; Wang, H.X.; Li, X.Q.; Zhu, Y.L. Effect of hydrolysis of tetraethyl orthosilicate (TEOS) on titanium distribution of TS-1 zeolite. *J. Fuel Chem. Technol.* **2022**, *50*, 1471–1479. [CrossRef]
26. Musić, S.; Filipović-Vinceković, N.; Sekovanić, L. Precipitation of amorphous SiO2 particles and their properties. *Braz. J. Chem. Eng.* **2011**, *28*, 89–94. [CrossRef]
27. Ortega, M.P.; López-Marín, L.M.; Millán-Chiu, B.; Manzano-Gayosso, P.; Acosta-Torres, L.S.; García-Contreras, R.; Manisekaran, R. Polymer mediated synthesis of cationic silver nanoparticles as an effective anti-fungal and anti-biofilm agent against Candida species. *Colloid Interface Sci. Commun.* **2021**, *43*, 100449. [CrossRef]
28. Rodriguez, A.F.R.; Rocha, C.O.; Piazza, R.D.; Dos Santos, C.C.; Morales, M.A.; Faria, F.S.E.D.V.; Marques, R.F.C. Synthesis, characterization and applications of maghemite beads functionalized with rabbit antibodies. *Nanotechnology* **2018**, *29*, 365701. [CrossRef]
29. An, G.S.; Choi, S.W.; Kim, T.G.; Shin, J.R.; Kim, Y.I.; Choi, S.C.; Jung, Y.G. Amino-functionalization of colloidal alumina particles for enhancement of the infiltration behavior in a silica-based ceramic core. *Ceram. Int.* **2017**, *43*, 157–161. [CrossRef]

Disclaimer/Publisher's Note: The statements, opinions and data contained in all publications are solely those of the individual author(s) and contributor(s) and not of MDPI and/or the editor(s). MDPI and/or the editor(s) disclaim responsibility for any injury to people or property resulting from any ideas, methods, instructions or products referred to in the content.